Dissociation of internal energy-selected methyl bromide ion revealed from threshold photoelectron-photoion coincidence velocity imaging

Xiaofeng Tang, Xiaoguo Zhou, Zhongfa Sun, Shilin Liu, Fuyi Liu, Liusi Sheng, and Bing Yan

Citation: The Journal of Chemical Physics **140**, 044312 (2014); doi: 10.1063/1.4862686
View online: http://dx.doi.org/10.1063/1.4862686
View Table of Contents: http://scitation.aip.org/content/aip/journal/jcp/140/4?ver=pdfcov
Published by the AIP Publishing

Dissociation of internal energy-selected methyl bromide ion revealed from threshold photoelectron-photoion coincidence velocity imaging

Xiaofeng Tang,[1,2] Xiaoguo Zhou,[1,3,a)] Zhongfa Sun,[1] Shilin Liu,[1,3] Fuyi Liu,[2] Liusi Sheng,[2] and Bing Yan[4,a)]

[1]*Hefei National Laboratory for Physical Sciences at the Microscale and Department of Chemical Physics, University of Science and Technology of China, Hefei 230026, China*
[2]*National Synchrotron Radiation Laboratory, University of Science and Technology of China, Hefei 230029, China*
[3]*Synergetic Innovation Center of Quantum Information & Quantum Physics, University of Science and Technology of China, Hefei, Anhui 230026, China*
[4]*Institute of Atomic and Molecular Physics, Jilin University, Changchun 130012, China*

(Received 8 November 2013; accepted 6 January 2014; published online 24 January 2014)

Dissociative photoionization of methyl bromide (CH_3Br) in an excitation energy range of 10.45–16.90 eV has been investigated by using threshold photoelectron-photoion coincidence (TPEPICO) velocity imaging. The coincident time-of-flight mass spectra indicate that the ground state X^2E of CH_3Br^+ is stable, and both A^2A_1 and B^2E ionic excited states are fully dissociative to produce the unique fragment ion of CH_3^+. From TPEPICO 3D time-sliced velocity images of CH_3^+ dissociated from specific state-selected CH_3Br^+ ion, kinetic energy release distribution (KERD) and angular distribution of CH_3^+ fragment ion are directly obtained. Both spin-orbit states of $Br(^2P)$ atom can be clearly observed in fast dissociation of $CH_3Br^+(A^2A_1)$ ion along C–Br rupture, while a KERD of Maxwell-Boltzmann profile is obtained in dissociation of $CH_3Br^+(B^2E)$ ion. With the aid of the re-calculated potential energy curves of CH_3Br^+ including spin-orbit coupling, dissociation mechanisms of CH_3Br^+ ion in A^2A_1 and B^2E states along C–Br rupture are revealed. For $CH_3Br^+(A^2A_1)$ ion, the $CH_3^+ + Br(^2P_{1/2})$ channel is occurred via an adiabatic dissociation by vibration, while the $Br(^2P_{3/2})$ formation is through vibronic coupling to the high vibrational level of X^2E state followed by rapid dissociation. C–Br bond breaking of $CH_3Br^+(B^2E)$ ion can occur via slow internal conversion to the excited vibrational level of the lower electronic states and then dissociation. © *2014 AIP Publishing LLC*. [http://dx.doi.org/10.1063/1.4862686]

I. INTRODUCTION

Methyl bromide (CH_3Br) is a trace gas with the largest abundance of bromine in the lower Earth's atmosphere and takes a considerable importance in the atmospheric and environmental sciences.[1] It is believed that CH_3Br plays a major role in the depletion of ozone in the stratosphere.[2,3] In addition, CH_3Br has attracted extensive attention in the past decades as a typical polyatomic molecule with C_{3V} symmetry to investigate unimolecular dissociation dynamics.[4]

The valence-shell electron configuration of neutral CH_3Br molecule with C_{3V} symmetry is $(1a_1)^2(2a_1)^2(1e)^4(3a_1)^2(2e)^4$,[5,6] where the nonbonding (2e) electron is of the halogen lone pairs, the $(3a_1)$ electron is associated with the C–Br bond and the (1e) electron belongs to the C–H bond. Stripping an electron from the outer orbitals, e.g., 2e, $3a_1$, and 1e, CH_3Br^+ ions in the X^2E, A^2A_1, and B^2E ionic states can be produced, respectively. The molecular structure of CH_3Br^+ ion was extensively studied by using vacuum UV absorption spectroscopy,[5,7] dipole (e,e) electron spectroscopy,[7] photoelectron spectroscopy (PES),[8–11] threshold photoelectron spectroscopy (TPES),[6,12] and pulsed field ionization photoelectron spectroscopy (PFI-PES).[13] The adiabatic and vertical ionization energies, and vibrational frequencies of the X^2E state were precisely determined. Moreover, a series of vibronic bands were observed, respectively, for both $^2E_{3/2}$ and $^2E_{1/2}$ spin-orbit states of X^2E,[13] while both A^2A_1 and B^2E excited electronic states did not exhibit any vibrational structure.

Using electron impact ionization[14–16] or photoionization,[6,17–19] many fragment ions, e.g., CH_2Br^+, CH_3^+, CH_2^+, Br^+, H_2^+, and HBr^+ were observed below 75 eV. Both CH_3^+ and CH_2Br^+ fragmentation channels were also observed in Penning ionization[20] and charge-exchange reactions experiments.[21] The accurate fragment appearance energies (AE) and the 0 K bond dissociation energies (BDE) for CH_3^+–Br rupture were measured by using threshold photoelectron-photoion coincidence (TPEPICO)[22] and high energy-resolution pulsed field ionization (PFI) photoelectron-photoion coincidence (PEPICO)[23] techniques. The values of $AE(CH_3^+)$ and $BDE(CH_3^+–Br)$ were determined as 12.834 ± 0.002 eV and 2.291 ± 0.002 eV, respectively.[23]

a)Authors to whom correspondence should be addressed. Electronic addresses: xzhou@ustc.edu.cn and yanbing@jlu.edu.cn.

For dissociation of CH_3Br^+ ion in the specific low-lying electronic excited states, CH_3^+ was the unique fragment ion of A^2A_1 and B^2E states in PEPICO measurement of Eland *et al.*[4] A small released kinetic energy was observed for the fragmentation process and rose slowly with available energy, which did not match the statistical distribution. However, CH_2Br^+ was also observed besides CH_3^+ fragment ion in the later PEPICO measurements of Lane and Powis.[24] Moreover, through fitting time-of-flight (TOF) profiles of CH_3^+ fragment ions, the released kinetic energies were roughly estimated as an approximate statistical distribution for C–Br rupture from both A^2A_1 and B^2E states. Apparently, the above two studies arrived at opposite conclusions. Recently, Wang *et al.*[25] generated CH_3Br^+ ion by (2 + 1) resonant enhanced multiphoton ionization (REMPI) and then dissociated it with an additional same photon of 3.60–3.72 eV (the energy is close to B^2E state). In the velocity image of CH_3^+ fragment, two dissociation channels to produce $Br(^2P_{3/2})$ and $Br(^2P_{1/2})$ were identified and an excitation of the umbrella vibration (v_2^+) of CH_3^+ was confirmed. Similarly, UV dissociation dynamics of CH_3Br^+ in 323–334 nm range (3.71–3.85 eV) were studied by Blanchet *et al.*[26] In the energy range of B^2E state, the v_4 degenerate bend of CH_3^+ was mostly populated within CH_3^+–Br rupture. Recently, Xi and Huang calculated the Br-loss and H-loss potential energy curves of CH_3Br^+ in the low-lying electronic states.[27] Potential wells along C–Br bond coordinate were found for X^2E, A^2A_1, and B^2E states, respectively. The dissociation of $CH_3Br^+(B^2E)$ ion was suggested to occur via internal conversion to X^2E ground state followed the statistically dissociation, while a directly dissociation by vibration was proposed for $CH_3Br^+(A^2A_1)$ ion in Franck-Condon region.

Although high energy-resolution velocity images of CH_3^+ were detected by Wang *et al.* and Blanchet *et al.*,[25,26] the excitation energies were located in the Franck-Condon gap of A^2A_1 and B^2E ionic states. Due to significant overlap between A^2A_1 and B^2E states, it is difficult to identify that the detected CH_3^+ fragments in these two experiments were produced in dissociation of A^2A_1 or B^2E states. More importantly, both previous coincidence experiments drew the opposite conclusions on statistical or direct dissociation of $CH_3Br^+(A^2A_1)$ ion,[4,24] as mentioned above. Therefore, the detailed dissociation mechanisms of CH_3Br^+ ion in specific A^2A_1 and B^2E states are still unclear. Moreover, the C–H rupture of CH_3Br^+ ion in A^2A_1 and B^2E states also needs to be re-checked, since Lane and Powis[24] detected CH_2Br^+ fragment but it was missing in another PEPICO[4] and ion-dissociation measurements.[25,26]

A novel TPEPICO velocity imaging setup[28] has been shown to be very powerful for investigating dissociative photoionization(DPI) of molecules.[29–33] Significantly different from the previous multiphoton ionization-dissociation experiments,[25,26] the CH_3Br^+ ion can be directly produced in specific electronic states via one-photon ionization within an excitation energy range of 10.45–16.90 eV. Consequently, the fragment ions dissociated from internal energy-selected $CH_3Br^+(A^2A_1$ or $B^2E)$ ion can be measured. Their kinetic energy release distribution (KERD) and angular distributions are acquired from the corresponding TPEPICO velocity image, and thus dissociation mechanism is proposed with the aid of theoretical calculation.

II. EXPERIMENTAL

All the experiments were carried out at the U14-A undulator beamline of National Synchrotron Radiation Laboratory in Hefei, China. The details of the beamline and TPEPICO velocity imaging spectrometer have been introduced previously,[28] and thus only a brief description is presented here.

A 6-m-long monochromator was used to disperse synchrotron radiation from 800 MeV electron storage ring, where a spherical grating with 370 grooves mm^{-1} was used to cover a photon energy range of 7.5–22.5 eV. In present experiments, both entrance and exit slits of the monochromator were kept at 80 μm, and hence the resolved power (E/ΔE) of photon energy was about 2000. A gas filter with noble gas was used to reduce higher-order harmonic radiation of the beamline.

Once photoionization, electron, and ion were pushed apart by a direct current extraction field of 14 V cm^{-1}, and both of their velocity images were obtained in the opposite directions. With a repelling electric field of focusing lens, electron image was dramatically magnified, e.g., electrons with 50 meV kinetic energy would produce a ~25-mm-diameter image. A mask with a 1-mm-diameter central hole located at the front of electron detector was used to sift zero-kinetic-energy electrons (so-called as threshold photoelectrons), and thus the contamination of energetic electrons can be efficiently suppressed. The detected threshold photoelectrons were amplified by a preamplifier (ORTEC, VT120C) and recorded by a multiscaler (FAST Comtec GmbH, P7888). The synchrotron photon flux was measured with a silicon photodiode in order to normalize threshold photoelectron spectroscopy. On the other direction, ions were projected onto the surface of MCPs (Burle, 40 mm diameter) backed by a phosphor screen. A thermoelectrically cooled charge-coupled-device camera (Andor, DU934N-BV) was used to record ion image on the screen. In a coincidence measurement, the detected threshold photoelectron provided a starting time for ion flight time, and a pulsed high voltage (DEI, PVX-4140) was applied at MCPs of ion detector as "mass gate" to select the target ion. The effective duration time of "mass gate" was kept as 60 ns when recording the time-sliced image.

Commercial CH_3Br/Ar (1:9) mixture gas with a stagnation pressure of 1.2 atm was introduced into the spectrometer through a home-made 30 μm diameter aperture. The continuous supersonic molecular beam (MB) was collimated by a 0.5-mm diameter skimmer and orthogonally intersected by synchrotron radiation at 10 cm downstream from the nozzle. The typical background pressure in the photoionization chamber was increased from 5×10^{-6} Pa to 1×10^{-4} Pa with the MB on.

III. RESULTS AND DISCUSSION

A. Threshold photoelectron spectrum of CH_3Br

Threshold photoelectron spectrum of CH_3Br in the excitation energy range of 10.45–16.90 eV has been measured

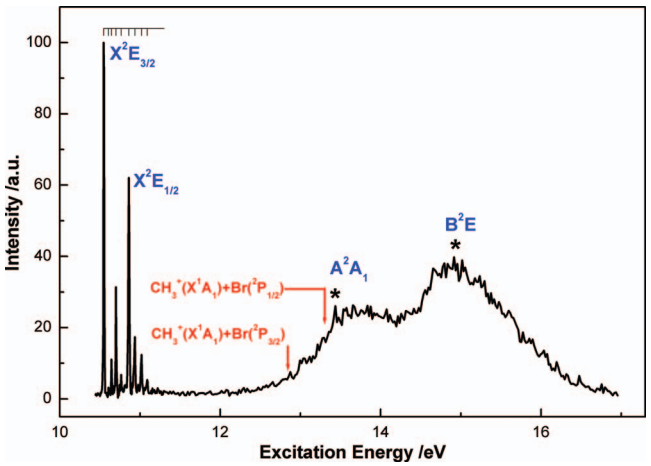

FIG. 1. Threshold photoelectron spectrum of CH_3Br in an excitation energy range of 10.45–16.90 eV. Two arrows indicate the dissociation limits of $CH_3^+(X^1A_1) + Br(^3P_{3/2})$ and $CH_3^+(X^1A_1) + Br(^3P_{1/2})$ channels, respectively. Two asterisks show the excitation energies of 13.440 and 14.940 eV, where TPEPICO velocity images of CH_3^+ fragments are recorded.

with a step size of 5 meV and presented in Figure 1. Three low-lying ionic states, X^2E, A^2A_1 and B^2E, are observed. For the ground electronic state of X^2E, a series of vibrational bands can be discerned. As shown in Figure 1, two strong peaks of X^2E located at 10.545 eV and 10.860 eV are assigned to the original bands of $^2E_{3/2}$ and $^2E_{1/2}$ spin-orbit states of X^2E, which is consistent with the previous assignments.[6,9,12] The other peaks between 10.5 eV and 11.3 eV can be attributed to the vibrational bands of the $^2E_{3/2}$ and $^2E_{1/2}$ states.

No vibrational structures are observed in Figure 1 for both A^2A_1 and B^2E excited electronic states. Moreover, no obvious spin-orbit and Jahn-Teller splitting can be observed for B^2E state, although their potential contributions probably make the tail of B^2E band towards the higher energy in Figure 1. The relative intensities of A^2A_1 and B^2E state in Figure 1 are slightly different to those in TPES observed by Locht *et al.*,[6] and the intensity of A^2A_1 state is weaker in the present spectrum. Since energetic electrons are efficiently suppressed in present TPEPICO spectrometer,[28] the intensities of these low-lying electronic states in Figure 1 should be more reliable.

B. TPEPICO time-of-flight mass spectra

Table I shows all energetically accessible dissociation channels of CH_3Br^+ in the present excitation energy range, where CH_3^+, CH_2Br^+, and Br^+ are the energetically accessible fragment ions. The lowest dissociation channel of C–H rupture is located at 12.77 eV[4] while the dissociation limit of $CH_3^+(X^1A_1) + Br(^2P_{3/2})$ is slightly higher at 12.834 eV.[23] Taking into account the spin-orbit splitting of $Br(^2P)$, the dissociation limit of $CH_3^+(X^1A_1) + Br(^2P_{1/2})$ is expected at 13.291 eV.

Fixing photon energy at 10.545 eV, $CH_3Br^+(X^2E_{3/2})$ ions are produced at the vibrational ground state. TPEPICO TOF mass spectrum was measured and presented in Figure 2(a). As the excitation energy is lower than all dissociation limits, only two mass peaks with 20.04 and 20.25 μs flight time

TABLE I. Adiabatic correlation dissociation limits of CH_3Br^+ ion in the low-lying ionic states.

Energy (eV)	Fragments	Adiabatic correlation ionic state of CH_3Br^+[a]
12.77[b]	$CH_2Br^+(X^1A') + H(^2S)$	X^2E ($^2A'$)
12.834[c]	$CH_3^+(X^1A_1) + Br(^2P_{3/2})$	X^2E ($^2A'$ and $^2A''$)
13.291[d]	$CH_3^+(X^1A_1) + Br(^2P_{1/2})$	A^2A_1 (A^2A')
14.42[b]	$CH_2^+(X^2\Pi) + HBr(X^1\Sigma^+)$	
14.78[b]	$CH_3(X^2A_2'') + Br^+(^3P_2)$	B^2E ($^2A'$ or $^2A''$)
15.17	$CH_3(X^2A_2'') + Br^+(^3P_1)$	$^2E_{3/2}$, $^2E_{1/2}$
15.26	$CH_3(X^2A_2'') + Br^+(^3P_0)$	$^2E_{1/2}$
15.67[b]	$HBr^+(X^2\Pi) + CH_2(X^3B_1)$	

[a]Spectral terms in parentheses are of C_s symmetry.
[b]From Ref. 4.
[c]From Ref. 23.
[d]Taking into account the spin-orbit splitting of $Br(^2P)$.

are clearly observed and attributed to $CH_3{}^{79}Br^+$ (m/z = 94) and $CH_3{}^{81}Br^+$ (m/z = 96) parent ions. Both intensities of $CH_3{}^{79}Br^+$ and $CH_3{}^{81}Br^+$ ions are almost equal, which is well consistent with the natural abundances of ^{79}Br and ^{81}Br isotopes. A width of less than 25 ns (full width at half magnitude, FWHM) is detected for both the CH_3Br^+ TOF peaks.

Figures 2(b) and 2(c) show TPEPICO TOF mass spectra at the excitation energies of 13.440 and 14.940 eV, which locate in the A^2A_1 and B^2E ionic states, respectively. Although the excitation energy is higher than dissociation limits of C–Br and C–H ruptures, a unique mass peak of CH_3^+ (m/z = 15) fragment ions is observed at TOF center of 7.92 μs, while no CH_2Br^+ fragment and CH_3Br^+ parent ions can be identified. The present conclusions are consistent with those observed by Eland *et al.*[4] and Olney *et al.*[7] However, H loss fragmentation was also observed in Lane and Powis's experiment[24] with He I photoionization. This inconsistency is probably caused by the different ionization processes between the present and previous experiments. As indicated in recent dissociation of ethanol ion[34] and formic acid ion,[35] the H-loss pathway usually has much slower rate than the channels of losing heavy fragments due to an activation barrier involved. Therefore, the

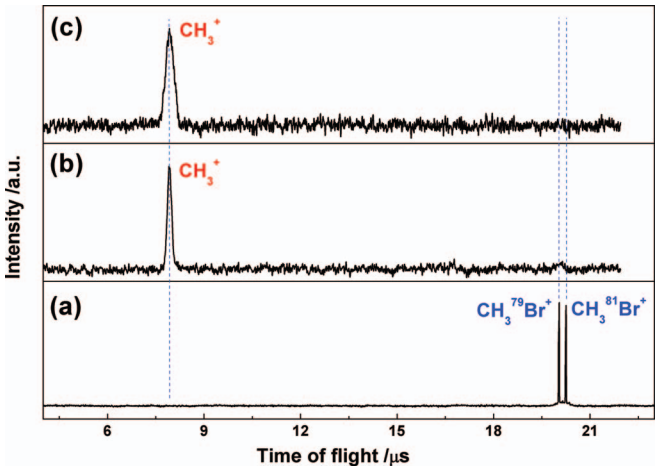

FIG. 2. TPEPICO TOF mass spectra for dissociative photoionization of CH_3Br at (a) 10.545 eV, (b) 13.440 eV, and (c) 14.940 eV.

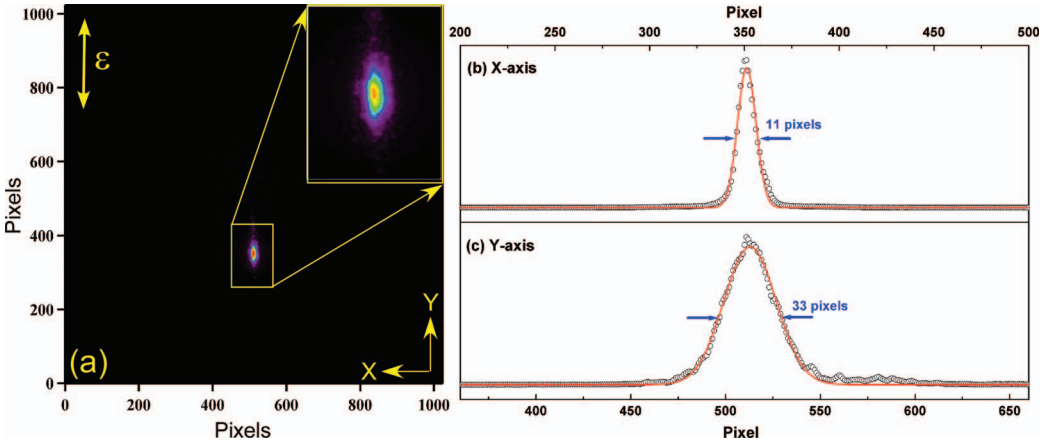

FIG. 3. (a) TPEPICO velocity image of $CH_3{}^{79}Br^+$ parent ion at 10.545 eV. Intensity of image along (b) *x*-axis and (c) *y*-axis, where black dots are experimental data and red lines are the least-square fitted results with Gaussian profiles.

Br-loss path of CH_3Br^+ would be more favorable, since a small barrier was confirmed indeed along the calculated H-loss potential energy curves by Xi and Huang.[27] However, the C–H rupture from CH_3Br^+ ion was suggested to proceed via an unknown dissociative state in Lane and Powis's experiment,[24] which led to the visible CH_2Br^+ fragmentation. Thus it is well possible that the He I photoionization favors the production of the dissociative state. Moreover, this difference caused by the different experimental methods was also observed between photoionization and electron impact of CH_3Cl.[32,36]

In addition, full widths of $CH_3{}^+$ peaks in Figures 2(b) and 2(c) are, respectively, expanded to be 370 and 640 ns, due to the released kinetic energy in dissociation. Therefore, the CH_3Br^+ ions in both A^2A_1 and B^2E states are fully dissociative to produce $CH_3{}^+$ and Br fragments within the present excitation energy range.

C. TPEPICO 3D time-sliced image of $CH_3{}^+$ dissociated from $CH_3Br^+(A^2A_1)$

Although KERD and mean kinetic energy of fragments can be roughly estimated from fitting the TOF profile of $CH_3{}^+$ fragment ions,[4,24,37] the detailed dissociation information may be buried. The kinetic energy distribution of fragment ions is expected to be accurately obtained from their velocity images of high energy resolution. However, according to a perpendicular configuration between the MB and ion flight directions in the spectrometer, the velocity spread of MB will inevitably reduce the energy-resolution of images along the MB direction.[28,32] Therefore, the recorded images should be handled prior to extracting the speed and angular distribution through a multistep data treatment scheme including quadrant symmetrization and deconvolution as described in Ref. 30.

As shown in the image of $CH_3{}^{79}Br^+$ parent ions at 10.545 eV of Figure 3, the raw image directly recorded in experiment is off-center indeed and broadened along the direction of MB. Using the intensity distribution of $CH_3{}^{79}Br^+$ ion image and the distance from centers of image and CCD, the parallel translational temperature of MB is calculated to be about 16 K, which will be used in the deconvolution of data.

TPEPICO three-dimensional time-sliced image of $CH_3{}^+$ fragment ions dissociated from $CH_3Br^+(A^2A_1)$ ions at 13.440 eV was recorded and presented in Figure 4(a). Two homocentric components are observed in the image, and both of them are slightly anisotropic and parallel to the electric vector ε of photon (as the vertical direction in Figure 4(a)). The speed distribution of $CH_3{}^+$ can be obtained based on its radial

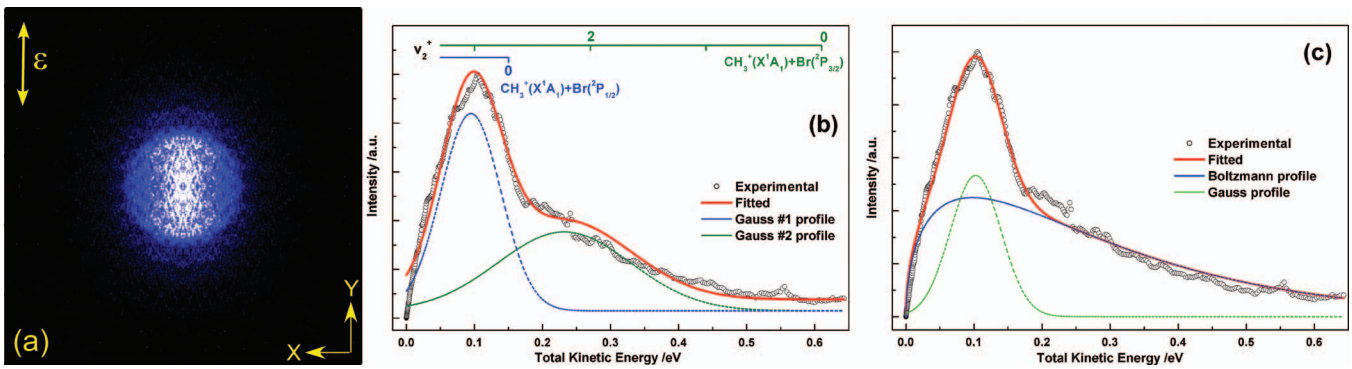

FIG. 4. (a) TPEPICO 3D time-sliced image of $CH_3{}^+$ fragment dissociated from $CH_3Br^+(A^2A_1)$ ions at 13.440 eV, (b) total kinetic energy release distributions with the fitted curve using two Gaussian profiles, and (c) fitting with a Gaussian and a Boltzmann profiles.

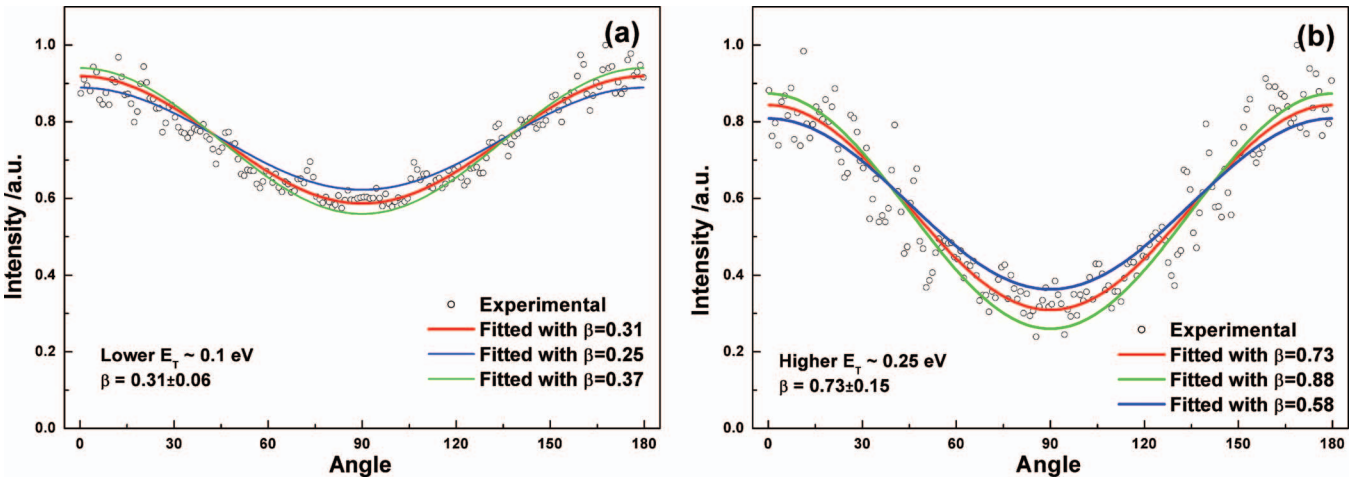

FIG. 5. Angular distributions of CH_3^+ dissociated from $CH_3Br^+(A^2A_1)$ ions at 13.440 eV for (a) the low kinetic energy component and (b) the high part, where the black dots are the experimental data and the red solid line is the fitted curves.

distribution. Subsequently taking into account conservation of linear momentum in center-of-mass frame, total KERD in dissociation of $CH_3Br^+(A^2A_1)$ ions at 13.440 eV is obtained and presented in Figure 4(b). Corresponding to the two parts of image, the total KERD can also be divided into two components, the low (~0.1 eV) and high (~0.25 eV) energy distributions. For a specific total released kinetic energy, the speed of CH_3^+ dissociated from $CH_3{}^{81}Br^+$ is only 0.2% higher than that from $CH_3{}^{79}Br^+$ ions. Thus we do not discriminate contributions from dissociation of $CH_3{}^{81}Br^+$ and $CH_3{}^{79}Br^+$ ions in Figure 4(b), since the energy resolution ΔE/E of the image is only about 3%.[28]

Although no vibrational structure can be discerned in the present total KERD, it is definitely different from the conclusion of statistical dissociation suggested by Lane and Powis.[24] Two possible candidates of dissociation mechanisms can be suggested for fitting the total KERD curve. One is done by using two Gaussian profiles as shown in Figure 4(b), while the other in Figure 4(c) is fitted with a Gaussian profile and a Boltzmann distribution. In principle the former indicates two fast dissociation mechanisms and the later implies a competition between a fast dissociation and a slow statistical fragmentation. Actually, the Boltzmann-like distribution in high kinetic energy region of the total KERD profile in Figure 4(c) may be the straightforward reason for Lane and Powis[24] to suggest the statistical dissociation mechanism of $CH_3Br^+(A^2A_1)$.

To affirm the true dissociation mechanism of $CH_3Br^+(A^2A_1)$ at 13.440 eV, a reasonable way is to compare angular distribution of fragments along two pathways. Anisotropic parameters β of statistical fragmentation are expected close to zero, while direct dissociation has a large β value (e.g., $\beta = 2$ for parallel and $\beta = -1$ for perpendicular distributions of diatomic molecule decomposition). From the image of Figure 4(a), angular distribution $I(\theta)$ of CH_3^+ fragment ions is obtained by integrating the intensity of image over a proper range of speed at each angle. Consequently, β value for a special dissociation process can be obtained by fitting the angular distribution $I(\theta)$ with the following formula:

$$I(\theta) = \frac{1}{4\pi}[1 + \beta \cdot P_2(\cos\theta)], \quad (1)$$

where θ is the angle between the recoil velocity of fragment and the electric vector of photon, and $P_2(\cos\theta)$ is the second-order Legendre polynomial. Thus angular distributions of CH_3^+ fragment ions of the low and high kinetic energy are shown in Figure 5. The fitting anisotropic parameters β are far from zero as 0.73 for the high kinetic energy component and 0.31 for the low part, respectively. Since both β values are far from zero, two rapid dissociation mechanisms for DPI process at 13.440 eV is more reasonable. Therefore the total KERD curve fitting with two Gaussian profiles in Figure 4(b) seems more reliable. Moreover, both β values are positive, indicating that dissociation of $CH_3Br^+(A^2A_1)$ ion has a parallel tendency along the polarization vector, which is similar to the conclusion in CH_3Br^+ decomposition in the wavelength range of 323–334 nm.[26]

At 13.440 eV, two dissociation channels of $CH_3^+(X^1A_1) + Br(^2P_{3/2})$ and $CH_3^+(X^1A_1) + Br(^2P_{1/2})$ are able to occur. Therefore two distributions of Gaussian profiles in the total KERD of Figure 4(b) can be straightforward attributed to the two C–Br rupture channels. The low kinetic energy distribution corresponds to the $CH_3^+(X^1A_1) + Br(^2P_{1/2})$ channel, while the high energy component is original from the contribution of $CH_3^+(X^1A_1) + Br(^2P_{3/2})$ fragmentation pathway. As shown in Figure 4(b), the Gaussian profile of the high kinetic energy exhibits the wider distribution than the low-energy one, but the corresponding branching ratio is very slightly lower as $Br(^2P_{3/2})/[Br(^2P_{1/2}) + Br(^2P_{3/2})] = 0.47$. Similar to the rapid dissociation of $CH_3Cl^+(A^1A_1)$,[32] the umbrella mode v_2^+ of CH_3^+ fragment is expected to be excited when the C–Br bond of $CH_3Br^+(A^2A_1)$ is broken. Taking the dissociation limit $D_0 = 12.834$ eV for the $CH_3^+(X^1A_1) + Br(^2P_{3/2})$ channel and $D_0 = 13.291$ eV for the $CH_3^+(X^1A_1) + Br(^2P_{1/2})$ channel from Table I, as well as the vibrational frequency $v_2^+ = 1380\ cm^{-1}$,[38,39] the possible vibrational state population of CH_3^+ fragment is assigned and shown in

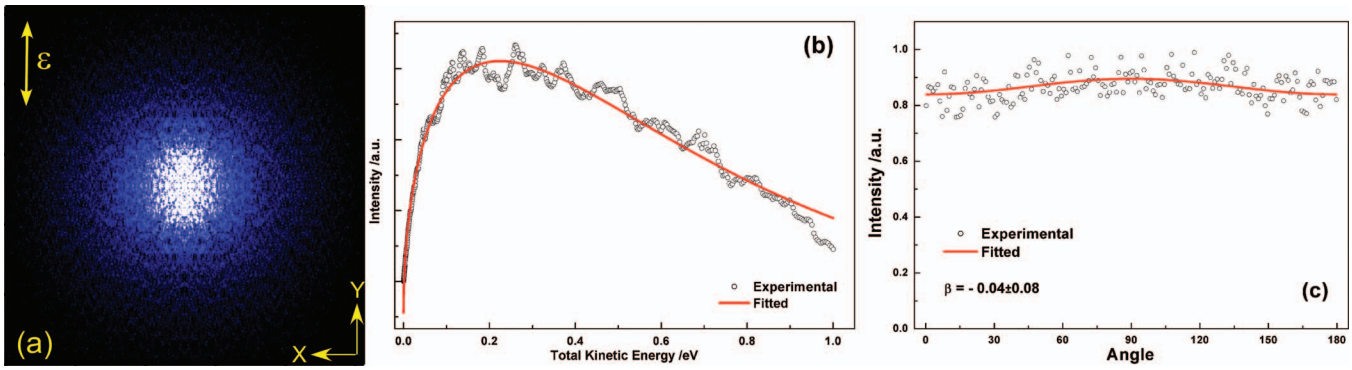

FIG. 6. (a) TPEPICO 3D time-sliced image of CH_3^+ fragment ions, (b) total kinetic energy release distribution, and (c) angular distribution in dissociation of $CH_3Br^+(B^2E)$ ions at 14.940 eV.

Figure 4(b) as well. Although no apparent vibrational structure is observed in the KERD curve, the vibrational population of CH_3^+ can be roughly assigned. The maximum vibrational quantum is located at $v_2^+ = 2$ for the $Br(^2P_{3/2})$ channel, while no umbrella vibrational excitation is obtained for the $Br(^2P_{1/2})$ channel at 13.440 eV. As shown in Figure 4(b), the higher rotational excitation of $CH_3^+(X^1A_1)$ fragment is observed along the $CH_3^+(X^1A_1) + Br(^2P_{1/2})$ channel, which is consistent with the lower β value for the $Br(^2P_{1/2})$ formation pathway.

D. TPEPICO 3D time-sliced image of CH_3^+ dissociated from $CH_3Br^+(B^2E)$

As indicated in Figures 1 and 2, $CH_3Br^+(B^2E)$ ions are produced at 14.940 eV and subsequently dissociate. TPEPICO 3D time-sliced image of CH_3^+ fragment ions at 14.940 eV is shown in Figure 6(a). Subsequently, the total KERD has been obtained and exhibited in Figure 6(b). The total KERD shows considerably wide and the most dominant distribution is located at low energy. As shown in Figure 6(b), the present total KERD can be fitted very well with a Maxwell-Boltzmann profile. Therefore fragmentation of $CH_3Br^+(B^2E)$ ions looks very slow via a statistical dissociation, which is in good agreement with the previous conclusions.[4,24]

Figure 6(c) shows the experimental and fitted angular distribution of CH_3^+ fragment ions at 14.940 eV. Obviously the angular distribution is almost isotropic with a fitted β value of −0.04, which is also consistent with the statistical dissociation mechanism. Therefore the $CH_3Br^+(B^2E)$ ion has a longer lifetime than that in A^2A_1 state, although its energy is much higher.

E. Br-loss potential energy curves of CH_3Br^+ ion in low-lying electronic states

To understand the dissociation mechanisms of CH_3Br^+ ions in A^2A_1 and B^2E states, the Br-loss potential energy curves of the low-lying electronic states of CH_3Br^+ ion were re-calculated. Compared with Xi and Huang's calculation,[27] more doublet and quartet electronic states were involved to study the possible interactions between them and A^2A_1 (or B^2E) states, and more significantly the spin-orbit coupling was included. The electronic structure computations were performed with Molpro2010 quantum chemistry package.[40,41] The geometry of CH_3Br^+ was constrained in C_{3v}, while the electronic states were calculated in C_s symmetry. Thus the degenerate E state in C_{3v} symmetry splits into $A'+A''$ states in C_s symmetry, the A_1 and A_2 states are corresponding to A' and A'' states, respectively. The pseudo-potential ECP28MDF in combination with (6s6p1d1f)/[4s4p1d1f] Gaussian basis set was used to describe Br atom.[42] For C and H atoms, Dunning's aug-cc-pVTZ basis sets[43] were used. The rigid potential energy cuts along C–Br bond distance were constructed with 38 single-point energies calculations. At each internuclear distance of C–Br bond, restricted Hartree-Fock method was used to generate starting molecular orbitals followed by state-average complete active space multiconfiguration self-consistent field (CASSCF)[44,45] computations. The active space consists of six electrons in six molecular orbitals in CASSCF calculations. Second-order perturbation theory based on CASSCF wavefunctions (CASPT2)[46] was used to evaluate the electron dynamical correlations. Subsequently, the spin-orbit coupling was calculated at each internuclear distance with state-interacting method. In the spin-orbital matrix calculations, the diagonal elements were replaced with CASPT2 energies.

The calculated potential energy curves of CH_3Br^+ ion are shown in Figure 7, where only doublet electronic states are shown. Due to convergence difficulty of multiconfiguration self-consistent field, geometry optimization and excitation energy calculations of B^2E ionic state were failed and excluded in Figure 7. Our another computation at the lower level of theory showed the similar Br-loss potential energy curve of B^2E to the Xi and Huang's conclusion,[27] which adiabatically correlated to a much higher dissociation limit of $CH_3^+(^3A'')+Br(^2P)$ than the present excitation energy range. Thus only a schematic curve of B^2E state is plotted in Figure 7 to compare with the X^2E and A^2A_1 states. It needs to be noted that only a little difference was observed between both $^2A'$ and $^2A''$ components along C–Br bond rupture for the double ^2E states. Therefore, the Jahn-Teller effect of X^2E electronic state is ignored in the following discussion of Br-loss mechanism of CH_3Br^+ ions. In addition, an energy shift exists between experimental and calculated dissociation limits,

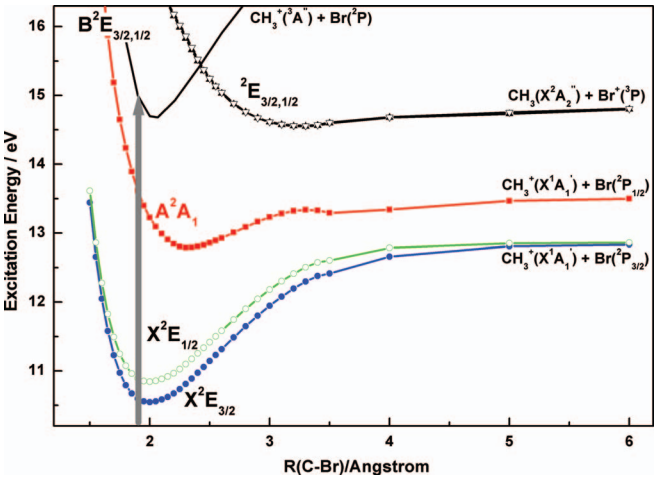

FIG. 7. Potential energy curves of the low-lying doublet electronic states of CH_3Br^+ ion along C–Br bond breaking, where that of B^2E is simply plotted by using the calculated energies at the lower level from Ref. 27. The gray arrow shows the Franck-Condon region of photoionization.

although the calculated energy difference between the electronic states remains good for spectroscopic data. In order to match the experimental dissociation limits, we slightly normalized the calculated curves in Figure 7.

The X^2E ionic state is adiabatically correlated to the lowest dissociation channel of $CH_3^+(X^1A_1)$ + $Br(^2P_{3/2})$, both for $^2A'$ and $^2A''$ Jahn-Teller states. For the A^2A_1 state of CH_3Br^+, a potential well is found along C–Br rupture with a depth of ~0.7 eV, which is different from the repulsive A^2A_1 state of CH_3F^+ and CH_3Cl^+ ions.[32] In the optimized equilibrium structure of $CH_3Br^+(A^2A_1)$ ion, C–Br bond length is 2.25 angstrom and thus the well deviates from the Franck-Condon region of photoionization (the optimized C–Br bond length is 1.968 angstrom in ground state of neutral CH_3Br). As indicated in Figure 7, $CH_3Br^+(A^2A_1)$ ion can quickly dissociate once it is produced by vertical photoionization. The adiabatic dissociation limit of A^2A_1 state is determined as $CH_3^+(X^1A_1)$+$Br(^2P_{1/2})$. The B^2E state is bound in Franck-Condon region. Its adiabatic dissociation products are the excited $CH_3^+(^3A'')$ and $Br(^2P)$ atom, and the corresponding energy is much higher than the present excitation energy.

F. Dissociation mechanisms of CH_3Br^+ ion in A^2A_1 and B^2E states

As observed in the present experiments, C–Br rupture of $CH_3Br^+(A^2A_1)$ ions can be occurred along two rapid dissociation processes. With the aid of potential energy curves in Figure 7, the detailed dissociation mechanism of CH_3Br^+ ion in A^2A_1 state can be derived. In the two dissociation channels, the $CH_3^+(X^1A_1)$ + $Br(^2P_{1/2})$ pathway is an adiabatic one by vibration. However, due to heavy mass effect the Br atom is moving slowly away, and the internal energy of $CH_3Br^+(A^2A_1)$ ion can be partially redistributed among all internal freedoms prior to full dissociation along the adiabatic pathway. Thus the rotation of CH_3^+ is expected to be excited, which agrees well with our measurement.

In the contrary, the $Br(^2P_{3/2})$ formation is proceeded through vibronic coupling to the high vibrational level of X^2E state followed by rapid dissociation, where deformation vibration of CH_3Br^+ with E symmetry is the most favorable to the coupling from A^2A_1 to X^2E state. Moreover, the large difference between geometry of CH_3^+ fragment ion (planar) and the CH_3 moiety (tetrahedral) of CH_3Br^+ would generally favor the umbrella vibration v_2^+ and/or in-plane bend v_4^+ (170 meV)[38,39] excitations of CH_3^+ in dissociation, which exactly matches the deformation vibration of CH_3Br^+ and is consistent with the present population distribution in Figure 4(b). Thus the vibronic coupling via deformation promotes the internal conversion from A^2A_1 state to X^2E state, and then CH_3Br^+ ion at the high vibronic level in X^2E state will adiabatically dissociate to produce $Br(^2P_{3/2})$ and $CH_3^+(X^1A_1)$ fragments.

In addition, the proportions of average kinetic energy over available energy at 13.440 eV for the two channels are much lower than the theoretical value of 0.83 calculated by using "impulsive mode", indicating that there is a tendency indeed to distribute more available energy into CH_3^+ internal state and not into translation. Furthermore, the angular distributions for two dissociation channels are positive at 13.440 eV as mentioned above, implying that both channels of $CH_3Br^+(A^2A_1)$ ion are parallel dissociations. Our present measurements agree with the conclusion of the UV dissociation dynamics of CH_3Br^+ in a wavelength range of 323–334 nm (3.71–3.85 eV),[26] although the excitation energy is much lower. As shown with the β values, the intermediate to produce $Br(^2P_{3/2})$ atom has slightly shorter dissociating time than $CH_3Br^+(A^2A_1)$ ion along the $CH_3^+(X^1A_1)$ + $Br(^2P_{1/2})$ channel. But the former is an indirect process, and hence its branching ratio strongly depends on the competition between the vibronic coupling and adiabatic dissociation. The competition results in the very close branching ratios for both $Br(^2P_{3/2})$ and $Br(^2P_{1/2})$ channels as mentioned above.

Since B^2E state is bound, the dissociation of $CH_3Br^+(B^2E)$ ions must occur via indirect pathways like internal conversion to the lower excited states or intersections with nearby repulsive states. However, a further computation using the atomic natural orbital (ANO) type Gaussian basis sets ANO-RCC[47,48] suggests all the doublet or quartet states near B^2E adiabatically correlate to the $CH_3(X^2A_2'')$+$Br^+(^3P)$ or the higher limits. Thus intersections between B^2E and nearby repulsive states could not cause the CH_3^+ fragmentation of $CH_3Br^+(B^2E)$ ion at 14.940 eV. On the other hand, two candidates of the lower electronic states for internal conversion at 14.940 eV are A^2A_1 and the high vibrational level of X^2E states, respectively. Since the subsequent dissociations from both A^2A_1 and the high vibrational states of X^2E states are very fast as discussed in dissociation of CH_3Br^+ ion at 13.440 eV, the statistical dissociation of $CH_3Br^+(B^2E)$ ion at 14.940 eV indicates that the internal conversion is slow as the rate-determined step in dissociation. Moreover, timescale of the internal conversion is longer than the period of molecular rotation.

IV. CONCLUSIONS

Utilizing the TPEPICO velocity imaging, dissociative photoionization of CH_3Br via the low-lying ionic electronic

states, X^2E, A^2A_1, and B^2E, has been investigated. TPES in the excitation energy range of 10.45–16.90 eV was recorded, where the spin-orbit splitting of X^2E ground state as well as its vibrational structure have been clearly discerned, while no vibrational structure are observed for both the A^2A_1 and B^2E excited states. As indicated in TPEPICO TOF mass spectra at 10.545 eV, 13.440 eV, and 14.940 eV, the X^2E ground state is stable while both A^2A_1 and B^2E states are fully dissociative. CH_3^+ is the unique fragment ion detected in the present excitation energy range.

TPEPICO 3D time-sliced velocity images of CH_3^+ fragment ion dissociated from CH_3Br^+ ion in A^2A_1 and B^2E states are measured, respectively. The total KERD and angular distribution of CH_3^+ are subsequently obtained. For dissociation of $CH_3Br^+(A^2A_1)$ ions, both the $CH_3^+(X^1A_1)$ + $Br(^2P_{3/2})$ and $CH_3^+(X^1A_1)$ + $Br(^2P_{1/2})$ dissociation channels are clearly discerned with the parallel angular distributions. With the aid of the re-calculated potential energy curves of CH_3Br^+ ion, the CH_3^+ formation pathway from dissociation of $CH_3Br^+(A^2A_1)$ ion includes two parallel mechanisms: the $CH_3^+(X^1A_1) + Br(^2P_{1/2})$ channel is directly adiabatic dissociation along its adiabatic Br-loss pathway, and the other is to produce $Br(^2P_{3/2})$ atom via vibronic coupling to the high vibrational level of X^2E state followed by rapid dissociation. Although the available energy is increased, the total KERD of CH_3^+ fragment dissociated from $CH_3Br^+(B^2E)$ exhibits an approximate Maxwell-Boltzmann profile, and the angular distribution is nearly isotropic. Therefore, a statistical dissociation is occurred for CH_3Br^+ ion in B^2E state at 14.940 eV. Based on the calculated potential energy curve along C–Br rupture, an internal conversion from B^2E to the lower electronic states (A^2A_1 or X^2E) seems to be the rate-determined step in dissociation. Moreover, timescale of the internal conversion is longer than the period of molecular rotation.

ACKNOWLEDGMENTS

The authors would like to appreciate the discussion with Professor Haifeng Xu and Mr. Xiaobin Shan's help in operating synchrotron radiation. The present work was supported by the National Natural Science Foundation of China (NSFC, Grant Nos. 21073173, 21027005, 21373194, and 21303177) and National Key Basic Research Special Foundation (NKBRSF, Grant Nos. 2013CB834602 and 2010CB923300).

[1]M. J. Molina, L. T. Molina, and C. E. Kolb, Annu. Rev. Phys. Chem. **47**, 327 (1996).
[2]A. Mellouki, R. K. Talukdar, A. M. Schmoltner, T. Gierczak, M. J. Mills, S. Solomon, and A. R. Ravishankara, Geophys. Res. Lett. **19**, 2059, doi:10.1029/92GL01612 (1992).
[3]J. S. Daniel, S. Solomon, R. W. Portmann, and R. R. Garcia, J. Geophys. Res., [Atmos.] **104**, 23871, doi:10.1029/1999JD900381 (1999).
[4]J. H. D. Eland, R. Frey, A. Kuestler, H. Schulte, and B. Brehm, Int. J. Mass Spectrom. Ion Process. **22**, 155 (1976).
[5]R. Locht, B. Leyh, H. W. Jochims, and H. Baumgartel, Chem. Phys. **317**, 73 (2005).
[6]R. Locht, B. Leyh, D. Dehareng, K. Hottmann, H. W. Jochims, and H. Baumgartel, Chem. Phys. **323**, 458 (2006).
[7]T. N. Olney, G. Cooper, W. F. Chan, G. R. Burton, C. E. Brion, and K. H. Tan, Chem. Phys. **218**, 127 (1997).
[8]J. L. Ragle, I. A. Stenhous, D. C. Frost, and C. A. McDowell, J. Chem. Phys. **53**, 178 (1970).
[9]L. Karlsson, R. Jadrny, L. Mattsson, F. T. Chau, and K. Siegbahn, Phys. Scr. **16**, 225 (1977).
[10]C. Utsunomiya, T. Kobayashi, and S. Nagakura, Bull. Chem. Soc. Jpn. **53**, 1216 (1980).
[11]W. von Niessen, L. Asbrink, and G. Bieri, J. Electron Spectrosc. Relat. Phenom. **26**, 173 (1982).
[12]B. Urban and V. E. Bondybey, J. Chem. Phys. **116**, 4938 (2002).
[13]X. Xing, P. Wang, B. Reed, S. J. Back, and C. Y. Ng, J. Phys. Chem. A **112**, 9277 (2008).
[14]H. Branson and C. Smith, J. Am. Chem. Soc. **75**, 4133 (1953).
[15]S. Tsuda and W. H. Hamill, J. Chem. Phys. **41**, 2713 (1964).
[16]S. Tsuda, C. E. Melton, and W. H. Hamill, J. Chem. Phys. **41**, 689 (1964).
[17]M. Krauss, J. A. Walker, and V. H. Dibeler, J. Res. Natl. Bur. Stand. **72A**, 281 (1968).
[18]M. L. Vestal and J. H. Futrell, Chem. Phys. Lett. **28**, 559 (1974).
[19]J. Zhang and J. Ma, Appl. Mech. Mater. **103**, 158 (2012).
[20]B. Brunetti, P. Candori, J. DeAndres, F. Pirani, M. Rosi, S. Falcinelli, and F. Vecchiocattivi, J. Phys. Chem. A **101**, 7505 (1997).
[21]S. Ikuta, K. Yoshihara, and S. Shiokawa, Bull. Chem. Soc. Jpn. **48**, 2134 (1975).
[22]B. P. Tsai, T. Baer, A. S. Werner, and S. F. Lin, J. Phys. Chem. **79**, 570 (1975).
[23]Y. Song, X. M. Qian, K. C. Lau, C. Y. Ng, J. B. Liu, and W. W. Chen, J. Chem. Phys. **115**, 4095 (2001).
[24]I. C. Lane and I. Powis, J. Phys. Chem. **97**, 5803 (1993).
[25]F. Y. Wang, M. L. Lipciuc, X. M. Yang, and T. N. Kitsopoulos, Phys. Chem. Chem. Phys. **11**, 2234 (2009).
[26]V. Blanchet, P. C. Samartzis, and A. M. Wodtke, J. Chem. Phys. **130**, 034304 (2009).
[27]H. W. Xi and M. B. Huang, J. Phys. Chem. A **110**, 8167 (2006).
[28]X. F. Tang, X. G. Zhou, M. L. Niu, S. L. Liu, J. D. Sun, X. B. Shan, F. Y. Liu, and L. S. Sheng, Rev. Sci. Instrum. **80**, 113101 (2009).
[29]X. F. Tang, M. L. Niu, X. G. Zhou, S. L. Liu, F. Y. Liu, X. B. Shan, and L. S. Sheng, J. Chem. Phys. **134**, 054312 (2011).
[30]X. F. Tang, X. G. Zhou, M. L. Niu, S. L. Liu, and L. S. Sheng, J. Phys. Chem. A **115**, 6339 (2011).
[31]X. F. Tang, X. G. Zhou, M. M. Wu, Y. Cai, S. L. Liu, and L. S. Sheng, J. Phys. Chem. A **116**, 9459 (2012).
[32]X. F. Tang, X. G. Zhou, M. M. Wu, S. L. Liu, F. Y. Liu, X. B. Shan, and L. S. Sheng, J. Chem. Phys. **136**, 034304 (2012).
[33]X. F. Tang, X. G. Zhou, M. M. Wu, Z. Gao, S. L. Liu, F. Y. Liu, X. B. Shan, and L. S. Sheng, J. Chem. Phys. **138**, 094306 (2013).
[34]A. Bodi, M. D. Brannock, B. Sztaray, and T. Baer, Phys. Chem. Chem. Phys. **14**, 16047 (2012).
[35]N. S. Shuman, M. Johnson, W. R. Stevens, M. E. Harding, J. F. Stanton, and T. Baer, J. Phys. Chem. A **114**, 10016 (2010).
[36]F. P. Lossing, Bull. Soc. Chim. Belg. **81**, 125 (1972).
[37]H. F. Xu, Y. Guo, Q. F. Li, Y. Shi, S. L. Liu, and X. X. Ma, J. Chem. Phys. **121**, 3069 (2004).
[38]X. H. Liu, R. L. Gross, and A. G. Suits, Science **294**, 2527 (2001).
[39]M. E. Jacox, J. Phys. Chem. Ref. Data **27**, 115 (1998).
[40]H. J. Werner, P. J. Knowles, G. Knizia, F. R. Manby, M. SchAutz *et al.*, MOLPRO, version 2012.1, a package of *ab initio* programs, 2012, see http://www.molpro.net.
[41]H. J. Werner, P. J. Knowles, G. Knizia, F. R. Manby, and M. Schutz, WIRES Comput. Mol. Sci. **2**, 242 (2012).
[42]H. Stoll, B. Metz, and M. Dolg, J. Comput. Chem. **23**, 767 (2002).
[43]T. H. Dunning, J. Chem. Phys. **90**, 1007 (1989).
[44]H. J. Werner and P. J. Knowles, J. Chem. Phys. **82**, 5053 (1985).
[45]P. J. Knowles and H. J. Werner, Chem. Phys. Lett. **115**, 259 (1985).
[46]P. Celani and H. J. Werner, J. Chem. Phys. **112**, 5546 (2000).
[47]P. O. Widmark, P. A. Malmqvist, and B. O. Roos, Theor. Chim. Acta **77**, 291 (1990).
[48]B. O. Roos, R. Lindh, P. A. Malmqvist, V. Veryazov, and P. O. Widmark, J. Phys. Chem. A **108**, 2851 (2004).